nature medicine

Directing mesenchymal stem cells to bone to augment bone formation and increase bone mass

Min Guan[1,5], Wei Yao[1,5], Ruiwu Liu[2], Kit S Lam[1,2], Jan Nolta[3], Junjing Jia[1], Brian Panganiban[4], Liping Meng[2], Ping Zhou[3], Mohammad Shahnazari[1], Robert O Ritchie[4] & Nancy E Lane[1]

Aging reduces the number of mesenchymal stem cells (MSCs) that can differentiate into osteoblasts in the bone marrow, which leads to impairment of osteogenesis. However, if MSCs could be directed toward osteogenic differentiation, they could be a viable therapeutic option for bone regeneration. We have developed a method to direct MSCs to the bone surface by attaching a synthetic high-affinity and specific peptidomimetic ligand (LLP2A) against integrin α4β1 on the MSC surface to a bisphosphonate (alendronate, Ale) that has a high affinity for bone. LLP2A-Ale induced MSC migration and osteogenic differentiation *in vitro*. A single intravenous injection of LLP2A-Ale increased trabecular bone formation and bone mass in both xenotransplantation studies and in immunocompetent mice. Additionally, LLP2A-Ale prevented trabecular bone loss after peak bone acquisition was achieved or as a result of estrogen deficiency. These results provide proof of principle that LLP2A-Ale can direct MSCs to the bone to form new bone and increase bone strength.

A decrease in the number of MSCs in the bone marrow with aging leads to reduced osteogenesis and bone formation[1–3]. Bone regeneration through induction of MSCs could promote osteogenesis and provide a rational therapeutic strategy for preventing age-related osteoporosis. Both autologous and allogeneic stem cells have been successfully infused for the treatment of degenerative heart or neuronal diseases or for injury repair[4–6]. However, systemic infusions of MSCs *in vivo* do not promote an osteogenic response in bone because of the inability of MSCs to home to the bone surface unless they have been genetically modified[7–10] or are infused after certain conditions, such as injuries[8,11,12]. This issue has become a major obstacle for MSC transplantation[13,14]. Even if the transplanted MSCs make it to the bone, they are usually observed engrafted in the upper metaphysis or the epiphysis or are within the bone marrow sinusoids or the Haversian system[14–16], rather than at the bone surface. Subsequently, the cells are removed from bone marrow within 4–8 weeks after infusion and do not show long-term engraftment[14,15,17].

MSCs within bone marrow have a multi-lineage potential and give rise to the following cell types: osteoblasts, chondrocytes and adipocytes[18,19]. MSCs undergo osteogenic differentiation in the bone marrow[9,20], and mobilization of the osteoblastic progenitors to the bone surface is a crucial step in osteoblast maturation and the formation of mineralized tissue[21,22]. Bone cells at all maturation stages are dependent on cell-matrix and cell-cell interactions[23,24]. Once the osteoblastic progenitors are directed to the bone surface, they synthesize a range of proteins, including osteocalcin, osteopontin, bone sialoprotein, osteonectin, type-I collagen and fibronectin, that will further enhance the adhesion and maturation of the osteoblasts[25,26]. These interactions are mostly mediated by transmembrane integrin receptors that primarily utilize an arginine, glycine, aspartate (ArgGlyAsp) sequence to identify and bind to specific ligands. MSCs express integrins α1, α2, α3, α4, α5, α6, α11 and β1 (ref. 27), whereas integrins with a β1 subunit are reported to be expressed in the osteoblasts[23,25]. Integrin α5 is required for MSC osteogenic differentiation[28], and overexpression of integrin α4 in MSCs has been reported to increase the homing of MSCs to bone[29]. These studies suggest that a therapeutic strategy for bone regeneration could be directed toward the integrins on the surface of the MSCs and could bring the MSCs to the bone surface.

We used a one-bead-one-compound combinatorial library method to develop a high-affinity and specific peptidomimetic ligand, LLP2A, against activated α4β1 integrin (half maximal inhibitory concentration (IC_{50}) = 2 pM)[30]. However, scrambled LLP2A ligand loses its affinity to α4β1 (ref. 30). We conjugated LLP2A to a bisphosphonate, alendronate, which served as a bone-seeking component, to direct both the cells and the compound to bone. We hypothesized this hybrid compound, LLP2A-Ale (**Supplementary Fig. 1**), could be used to direct MSCs to bone and augment bone formation.

RESULTS

General *in vivo* and *in vitro* effects

We treated mice with a wide range of doses of LLP2A-Ale (0.03–2 nmol) and did not observe organ toxicity at any of the doses, as evaluated by standard measurements of weight, kidney and liver function and calcium metabolism. In addition, we did not observe extraskeletal calcifications in mice treated with either LLP2A or LLP2A-Ale.

[1]Musculoskeletal Research Group, Department of Internal Medicine, University of California at Davis Medical Center, Sacramento, California, USA. [2]Department of Biochemistry and Molecular Medicine, University of California at Davis Medical Center, Sacramento, California, USA. [3]Department of Internal Medicine, Stem Cell Program and Institute for Regenerative Cures, University of California at Davis Medical Center, Sacramento, California, USA. [4]Department of Materials Science and Engineering, University of California at Berkeley, Berkeley, California, USA. [5]These authors contributed equally to this work. Correspondence should be addressed to W.Y. (wei.yao@ucdmc.ucdavis.edu).

Received 8 March 2011; accepted 4 August 2011; published online 5 February 2012; doi:10.1038/nm.2665

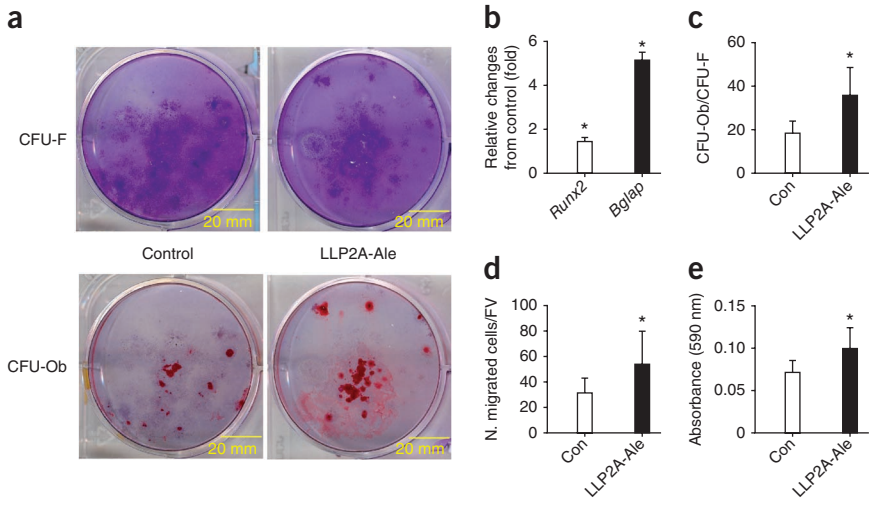

Figure 1 LLP2A-Ale increases MSC migration and bone marrow stromal cell (BMSC) osteoblastic differentiation. (**a**) Representative plates for the primary BMSCs that were cultured in osteogenic medium (control) or with LLP2A-Ale. Total colony forming units (CFU-F) stained with crystal violet and osteoblastic units (CFU-Ob) stained with Alizarin Red in the same plates. (**b**) Relative *Runx2* and *Bglap* expression at day 14 of the culture. (**c**) Transwell assays for the migration of mouse MSCs cultured for 10 h in control serum-free medium (con) or in serum-free medium with the addition of LLP2A-Ale. (**d**,**e**) The migrated cells were counted (**d**), and the crystal violet staining was eluted and read at an optical density of 590 nm (**e**). N. migrated cells/FV, number of migrated cells per field of view. $^{*}P < 0.05$ by paired *t* test for BMSCs cultured in LLP2A-Ale compared to those cultured in control. All the experiments were done in triplicate. Data are mean ± s.d.

We used color-coded peptide beads (rainbow beads) to semi-quantitatively determine the integrin profiles of MSCs undergoing osteogenic differentiation[31]. We found that the α4β1 integrin was highly expressed in the osteoprogenitor cells and had a high affinity for LLP2A (**Supplementary Fig. 2**). Treatment with LLP2A-Ale increased both the number of MSCs that differentiated into osteoblasts (**Fig. 1a–c**) as well as the migration of the MSCs (**Fig. 1d,e**), but did not affect their chondrogenic or adipogenic potentials.

LLP2A-Ale increases the bone homing and retention of MSCs

To determine whether LLP2A-Ale could direct transplanted MSCs to bone, we performed a xenotransplantation study. We intravenously (i.v.) injected human MSCs (huMSCs) or huMSCs plus LLP2A-Ale into nonobese diabetic (NOD)/severe combined immunodeficiency (SCID)/mucopolysaccharidosis type VII (MPS VII) mice. Twenty-four hours after the i.v. injections, we observed a number of huMSCs adjacent to the periosteal, endocortical and trabecular bone surfaces in the lumbar vertebral bodies (LVB) of the mice co-injected with LLP2A-Ale and huMSCs but not of the mice injected with huMSCs only (**Fig. 2a**).

At 3 weeks after injection, we observed huMSC cells adjacent to the bone surface and embedded within the bone matrix in the mice treated with huMSC and LLP2A-Ale but not in those treated with huMSCs only, suggesting that there was retention of the transplanted huMSCs (**Supplementary Fig. 3a**) in the bone of the former group. We observed higher concentrations of procollagen type I amino-terminal prepeptide (P1NP), an early osteoblast differentiation marker, in the mice treated with LLP2A-Ale + huMSCs compared to

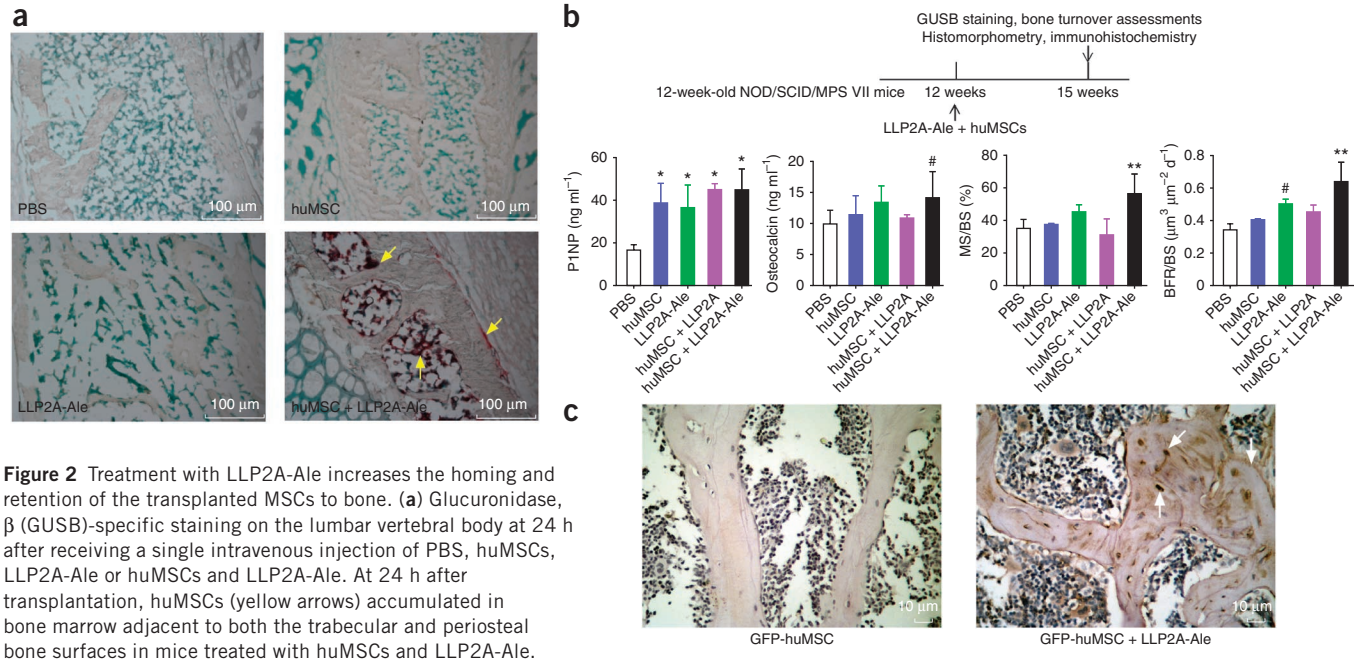

Figure 2 Treatment with LLP2A-Ale increases the homing and retention of the transplanted MSCs to bone. (**a**) Glucuronidase, β (GUSB)-specific staining on the lumbar vertebral body at 24 h after receiving a single intravenous injection of PBS, huMSCs, LLP2A-Ale or huMSCs and LLP2A-Ale. At 24 h after transplantation, huMSCs (yellow arrows) accumulated in bone marrow adjacent to both the trabecular and periosteal bone surfaces in mice treated with huMSCs and LLP2A-Ale. (**b**) Serum bone turnover markers and bone formation measured at the fifth LVB 3 weeks after injection and MSC transplantation. MS/BS, mineralizing surface; BFR/BS, bone surface-based bone formation rate. (**c**) Representative images from mice that received one single intravenous dose of LLP2A-Ale and GFP-MSC or GFP-MSC alone. Cells positive for GFP (stained brown) are sparse within bone marrow adjacent to the trabecular bone surface and within the bone matrix (white arrows) in the mice treated with GFP-MSC and LLP2A-Ale. $^{*}P < 0.05$ compared to the PBS group; $^{\#}P < 0.05$ compared to both the PBS and huMSC groups; $^{**}P < 0.05$ compared to the PBS, huMSC and huMSC + LLP2A groups by Kruskal-Wallis test. Data are mean ± s.d.

mice treated with huMSCs only. The concentrations of osteocalcin, an osteoblast maturation marker, and the bone formation parameters were higher in mice treated with LLP2A-Ale and those treated with huMSCs + LLP2A-Ale compared to the mice treated with PBS or huMSCs only (**Fig. 2b**).

In mice that we treated with GFP-labeled mouse MSCs or with LLP2A-Ale, the mice given the GFP-labeled mouse MSCs + LLP2A-Ale combination treatment showed higher numbers of the GFP-positive osteoblasts and osteocytes in both their trabecular (**Fig. 2c**) and cortical bone regions (**Supplementary Fig. 3b**) of the LVB of these mice at

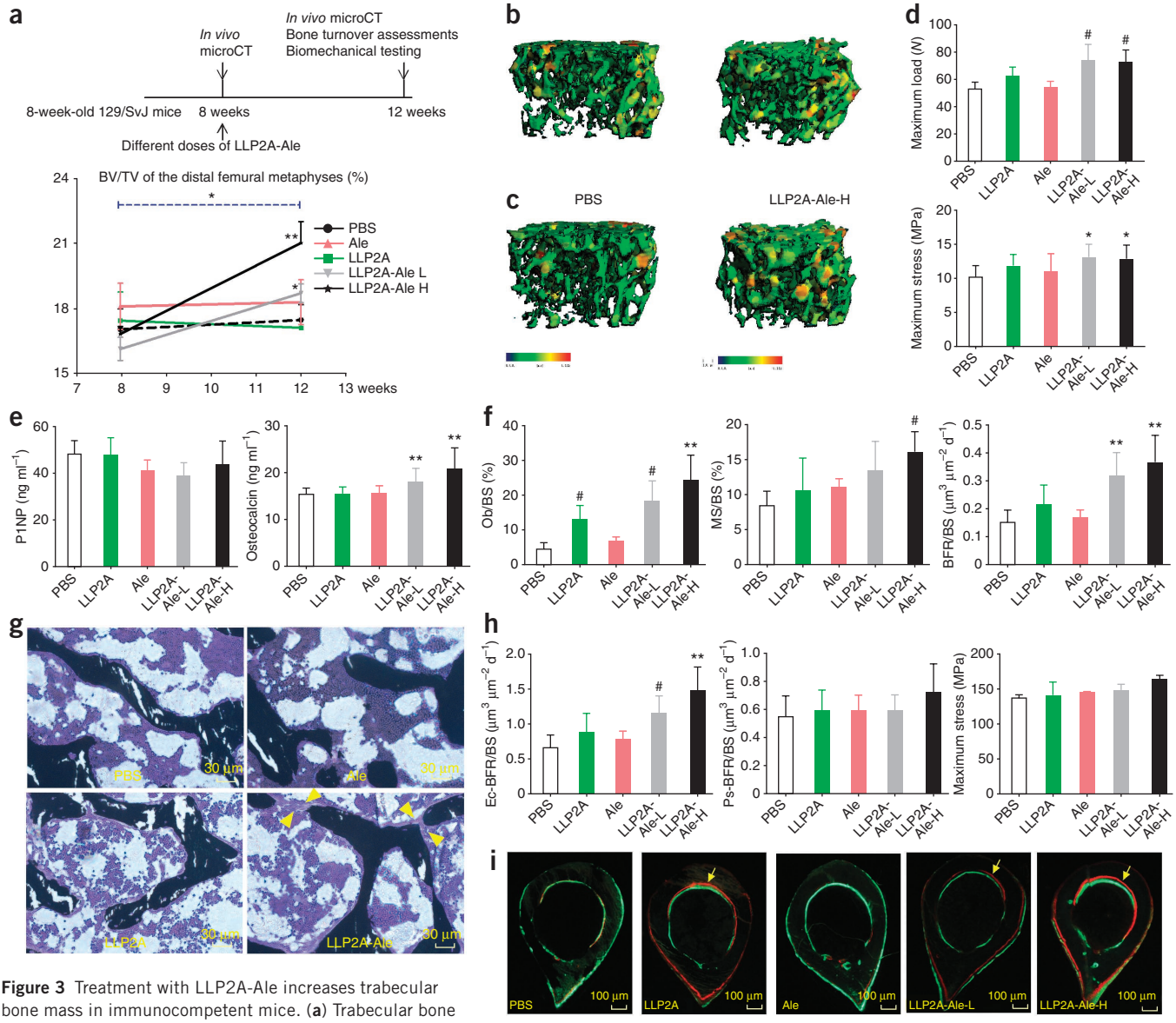

Figure 3 Treatment with LLP2A-Ale increases trabecular bone mass in immunocompetent mice. (**a**) Trabecular bone volume compared to the total tissue volume (BV/TV) measured by repeated *in vivo* microCT in 8-week-old female 129/SvJ mice. L, low dose; H, high dose. (**b**,**c**) Representative three-dimensional thickness maps from micro computed tomography (microCT) scans of trabecular bone from the distal femur metaphyses of the mice at baseline (8 weeks of age) (**b**) and from the same mice and at the same bone sites 4 weeks after a single injection of PBS or a high dose of LLP2A-Ale (LLP2A-Ale-H) (12 weeks of age) (**c**). The width of the trabecular is color coded, with the blue-green color indicating thin trabeculae and the yellow-red color indicating thick trabeculae. (**d**) Maximum load and maximum stress of the sixth lumbar vertebral bodies in mice at 12 weeks of age, 4 weeks after one injection of the agents indicated on the *x* axis. LLP2A-Ale-L, low dose of LLP2A-Ale; N, newton; MPa, megapascal. (**e**) Bone turnover markers measured from the serum of the mice treated with each indicated agent. (**f**) Surface-based bone histomorphometry was performed on the right distal femurs of mice from each indicated treatment group. Ob/BS, osteoblast surface. (**g**) Representative images from the trabecular bone of the distal femurs of the mice from the indicated treatment groups. The yellow arrowheads point to the osteoblastic bridges between the trabeculae in an LLP2A-Ale–treated mouse. (**h**) Surface-based bone histomorphometry was performed at the endosteal surface (Ec) and the periosteal surface (Ps) 4 weeks after the injections. Measurements of the maximum stress of the femurs were taken 4 weeks after the injections. (**i**) Representative cross sections of the tibial shafts from mice treated with PBS, LLP2A-Ale, a high dose of LLP2A-Ale or a low dose of LLP2A-Ale. The yellow arrows point to double-labeled bone surfaces. $^{*}P < 0.05$ compared to the PBS group; $^{\#}P < 0.05$ compared to both the PBS and huMSC groups; $^{**}P < 0.05$ compared to the PBS, huMSC and huMSC + LLP2A groups. Repeated measures analysis of variance followed by Bonferroni *post hoc* testing was used to analyze the *in vivo* microCT measurement in **a**. A nonparametric Kruskal-Wallis test was used for the parameters presented in **d**, **e**, **f** and **h**. Data are mean ± s.d.

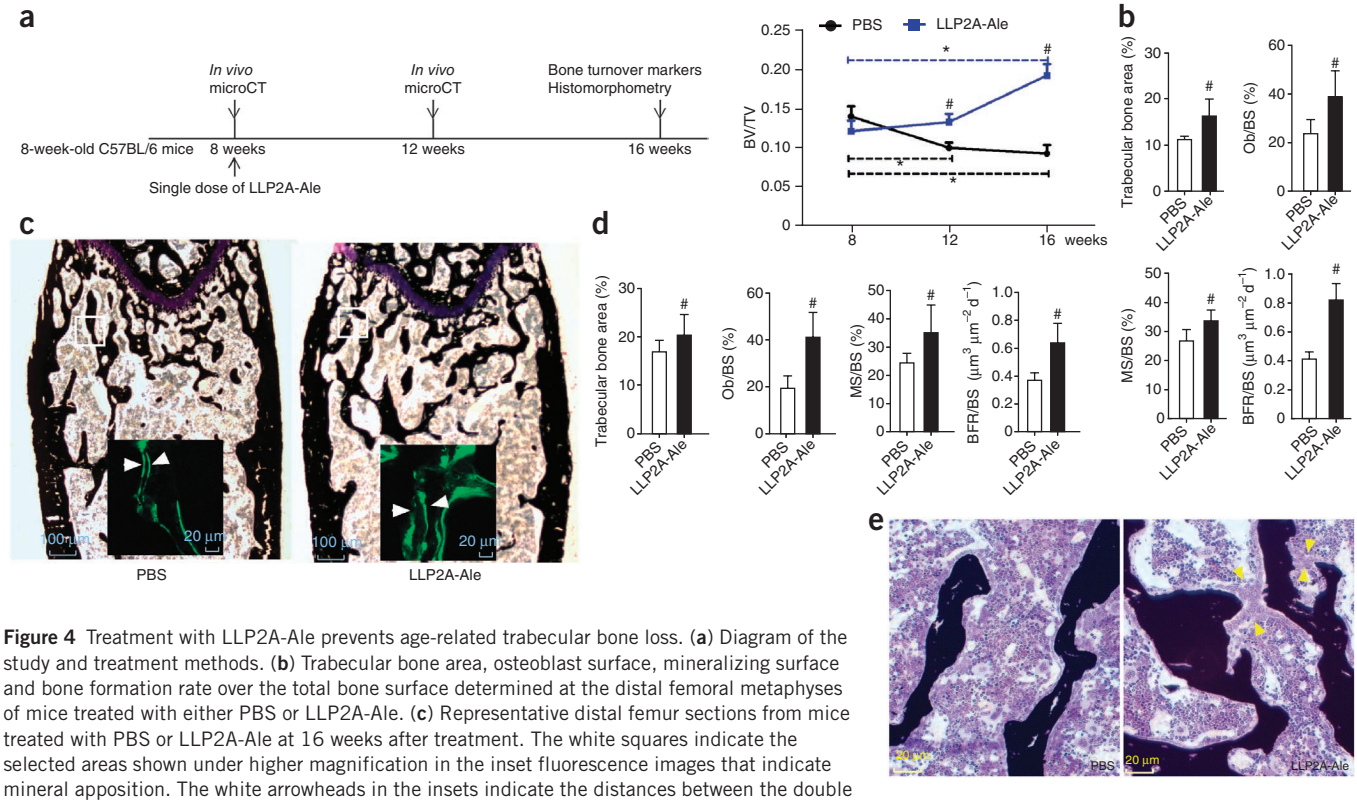

Figure 4 Treatment with LLP2A-Ale prevents age-related trabecular bone loss. (**a**) Diagram of the study and treatment methods. (**b**) Trabecular bone area, osteoblast surface, mineralizing surface and bone formation rate over the total bone surface determined at the distal femoral metaphyses of mice treated with either PBS or LLP2A-Ale. (**c**) Representative distal femur sections from mice treated with PBS or LLP2A-Ale at 16 weeks after treatment. The white squares indicate the selected areas shown under higher magnification in the inset fluorescence images that indicate mineral apposition. The white arrowheads in the insets indicate the distances between the double labels. (**d**) Trabecular bone area, osteoblast surface, mineralizing surface and bone formation rate compared to total bone surface performed at the fifth LVB sections from mice treated with PBS or LLP2A-Ale at 16 weeks of age (8 weeks after treatment). (**e**) Representative images taken from the trabecular bone at the fifth LVB. The yellow arrowheads point to the osteoblastic bridges in a mouse treated with LLP2A-Ale. $^{\#}P < 0.05$ compared to treatment with PBS at the same time point (either 8 or 16 weeks of age). $^{*}P < 0.05$ compared to baseline. Data are mean ± s.d.

3 weeks after injection. Collectively, these data show that LLP2A-Ale can direct transplanted MSCs to bone, increase the homing and retention of MSCs to bone and enhance endosteal and periosteal bone formation in a xenotransplantation model.

LLP2A-Ale augments bone formation in immunocompetent mice

To determine whether LLP2A-Ale could augment endogenous bone formation in immunocompetent mice without MSC transplantation, we used 2-month-old female 129/SvJ mice that received two doses of LLP2A-Ale, representing the effective dose compared to the placebo, LLP2A or Ale treatments and the maximum anabolic dose in our dose-finding studies. Two days after the i.v. injections, the cell populations expressing LLP2A, runt related transcription factor 2 (Runx2) (a gene marker for osteoblast maturation) and bromodeoxyuridine (Brdu) (a thymidine analog that is used in the detection of cell proliferation) were primarily located within the bone marrow in the LLP2A-treated mice but were located at the bone surface in the mice treated with LLP2A-Ale (**Supplementary Fig. 4**). The LLP2A and Brdu-positive cell populations were not detectable in the LVB at 21 d after injection in mice either injected with LLP2A or LLP2A-Ale.

Treatment with both doses of LLP2A-Ale induced a higher distal femoral trabecular bone volume (measured as trabecular bone volume (BV)/tissue volume (TV)) and thickness compared to baseline (**Fig. 3a–c**), with a corresponding greater maximum load and strength of the LVB in mice treated with LLP2A-Ale compared to mice treated with PBS, aledronate or LLP2A alone at 12 weeks after treatment (**Fig. 3d**). At 12 weeks after treatment, LLP2A-Ale dose-dependently resulted in a higher concentration of osteocalcin (**Fig. 3e**) and the surface-based bone-formation parameters at the distal femur in the LLP2A-Ale treated mice as compared to the groups treated with PBS or Ale only (**Fig. 3f**). More notably, LLP2A-Ale treatment increased the parameter of the osteoblast surface and formed bridges between adjacent trabeculae (**Fig. 3g**). Bone-formation rates on the endocortical surfaces of the tibial shafts were higher in mice that received LLP2A or LLP2A-Ale as compared to mice that received PBS or Ale (**Fig. 3h,i**).

LLP2A-Ale prevents trabecular bone loss in osteopenia mice

C57BL/6 mice usually achieve their peak bone mass by 6–8 weeks of age, and this peak is followed by an approximately 50% decline in both bone formation and bone mass at between 2 and 4 months of age[32,33]. Treatment with LLP2A-Ale in C57BL/6 mice prevented age-related trabecular bone loss after peak bone acquisition was achieved (**Fig. 4a**), with higher amounts of bone-formation parameters being present at the distal femur (**Fig. 4b,c**) as well as at the LVB in these mice compared to mice treated with PBS (**Fig. 4d,e**). We observed osteoblast bridges at both of these trabecular bone sites (**Fig. 4e**) in LLP2A-Ale–treated mice. These data suggest that one i.v. injection of LLP2A-Ale prevented age-related reductions in trabecular bone mass and bone formation for up to 8 weeks after injection in C57BL/6 mice.

To determine whether LLP2A-Ale could prevent bone loss in a disease state, we treated 10-week-old ovariectomized (OVX) mice with PBS, Ale, LLP2A, LLP2A-Ale or parathyroid hormone (PTH) 2 weeks after OVX (**Fig. 5a**). LLP2A-Ale treatment induced a larger osteoblast surface and a larger mineralizing surface, as well a higher bone-formation rate per total bone surface at the LVB in

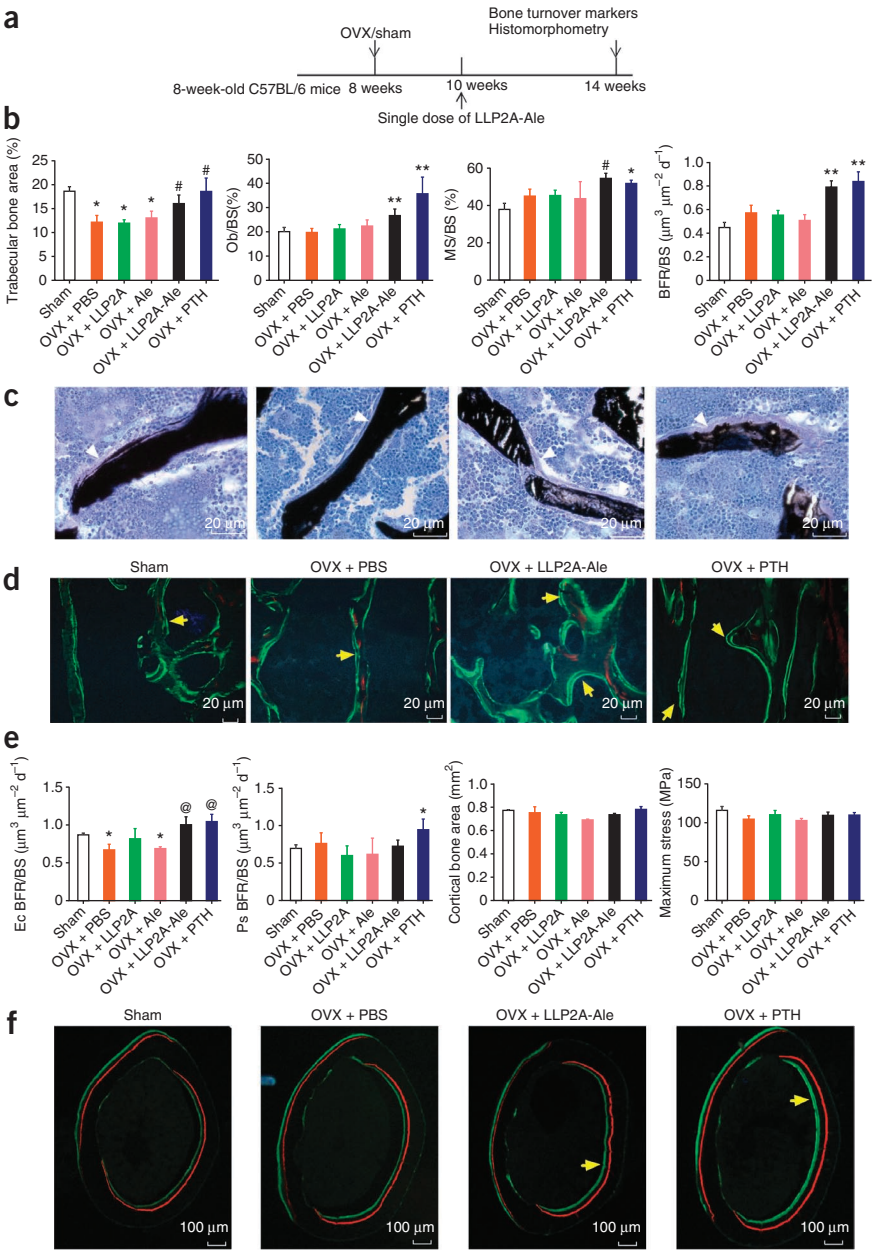

Figure 5 Treatment with LLP2A-Ale partially prevents trabecular bone loss and increases endosteal bone formation in OVX mice. (**a**) Diagram of the study and treatment methods. OVX/sham, mice were either ovariectomized or sham treated at this time point. $n = 6–8$ mice per group. (**b**) Histomorphometric analyses of the fifth LVBs from mice in each indicated treatment group, including analyses of the trabecular bone area, osteoblast surface, mineralizing surface and bone formation rate compared to the total bone surface. (**c**) Representative images from the trabecular bone at the fifth LVBs of the mice in each indicated treatment group. The white arrowheads point to the osteoblasts. (**d**) Representative fluorescent images from the trabecular bone at the fifth lumbar vertebral trabeculae of the mice from each indicated treatment group. The yellow arrows point to double-labeled trabecular bone surfaces. (**e**) Histomorphometry analyses of the right mid-femurs of mice from the indicated treatment groups, including analyses of bone formation at the endosteal or periosteal bone surfaces and cortical bone thickness. (**f**) Representative images from the mid-femur sections from mice in each indicated treatment group. The yellow arrows point to double-labeled endocortical bone surfaces. $^{*}P < 0.05$ compared to the PBS group; $^{\#}P < 0.05$ compared to both the PBS and LLP2A groups; $^{**}P < 0.05$ compared to the PBS, LLP2A and Ale groups; $^{@}P < 0.05$ compared to both the PBS and Ale groups. A nonparametric Kruskal-Wallis test was used for all comparisons. Data are mean ± s.d.

treated mice compared to the groups treated with PBS, Ale or LLP2A (**Fig. 5b–d**). Mice treated with either LLP2A-Ale or PTH had more endocortical bone formation compared to the mice treated with PBS or Ale (**Fig. 5e,f**). Cortical bone thickness and maximum stress were not significantly altered by OVX or by treatment with Ale, LLP2A, one single i.v. injection of LLP2A-Ale or 4 weeks of PTH (**Fig. 5e**). These data suggest an activation of endosteal bone formation by LLP2A-Ale that is comparable to that by PTH in this acute estrogen deficiency model.

DISCUSSION

MSCs are precursors of osteoblasts. MSCs do not readily migrate to the bone, and this creates a major obstacle for the use of MSCs for bone regeneration. We have developed a ligand that targets integrin α4β1, a protein that is highly expressed by MSCs undergoing osteoblast differentiation. Instead of using genetically modified MSCs, we attached LLP2A to a bisphosphonate (Ale) to guide the MSCs to the bone surface. Bisphosphonates are prescribed to reduce bone resorption and improve bone strength. Because we used approximately one-tenth of the therapeutic dose of Ale in our compound, we did not observe any anti-resorptive effects as a result of treatment. We observed an uncoupling of bone remodeling with bone formation and no marked changes in bone resorption during this short-term study period. This uncoupling of bone remodeling in favor of bone formation is also observed in short-term treatment with the anabolic agent human PTH (hPTH) (1-34)[34]. We hypothesized that we would also see a return to a coupling of bone turnover with this intervention after a longer treatment period. Additionally, the Ale concentrations that we used in these studies did not suppress TGF-β1 secretion (**Supplementary Fig. 5**), a growth factor that is crucial for coupling bone resorption and endogenous stem-cell recruitment to bone[35].

In our xenotransplantation model, LLP2A-Ale increased homing and retention of the transplanted MSCs to bone, which indicates a breakthrough in using transplanted MSCs to augment bone formation. We found the transplanted human or mouse MSCs embedded in the bone matrix as osteocytes or adjacent to the bone surface as osteoblasts. In addition to increasing bone formation rates at both the endocortical and trabecular surfaces, the periosteal bone formation rate also increased after MSC transplantation and after treatment with LLP2A-Ale. This is notable, as the total cross-sectional area increase as a result of periosteal expansion is the most important determinant of

bone strength[36]. Our finding that LLP2A-Ale can direct transplanted human MSCs to the bone is of major importance. This approach provides a means to overcome a major obstacle of using MSCs in the treatment of bone degenerative diseases and, as such, may be a new treatment option for osteoporosis.

Further, LLP2A-Ale might also increase endogenous MSC osteoblast differentiation and augment bone formation. We could not directly track the endogenous MSCs lineage commitment to osteoblasts, as there is no single marker that would allow us to define or track the migration of the endogenous MSCs to bone or their osteoblast differentiation *in vivo*. However, we were able to partially overcome this limitation by using control groups that we administered equivalent doses of Ale and LLP2A. Because LLP2A is a specific ligand for activated α4β1 integrin, our findings support the previous report that targeting α4 alone could increase the homing of MSCs to bone[37]. However, LLP2A by itself did not induce any marked changes in the bone architectures. In contrast, LLP2A-Ale enhanced osteoblast activities, as evidenced by the increased osteocalcin concentrations and increased bone formation in response to treatment that were primarily seen at the trabecular and endocortical bone surfaces that are in close contact with the bone marrow. Treatment with LLP2A-Ale not only increased the vertebral maximum load but also increased maximum bone stress, a parameter that is independent of bone shape, suggesting LLP2A-Ale treatment increased bone quality in addition to the observed increase in bone mass. Similarly, treatment with LLP2A-Ale prevented trabecular bone loss after peak bone mass had been achieved in C57BL/6 mice and partially prevented the rapid trabecular bone loss that is induced by OVX in these mice. Collectively, our findings show that LLP2A-Ale might be able to increase the migration of endogenous MSCs to bone, stimulate osteoblastic differentiation, augment bone formation and increase bone mass in young mice, as well as prevent trabecular bone losses associated with aging or estrogen deficiency. These results differ from what we observed in NOD/SCID/MPS VII mice that we treated with huMSCs and LLP2A-Ale, in which the combination treatment increased periosteal bone formation. This may have been a result of the lack of periosteal effects by LLP2A-Ale itself, the combination treatment may require more than one injection or a longer treatment period to achieve cortical bone responses.

In summary, we have shown that LLP2A-Ale augments endogenous bone formation and directs the transplanted MSCs to the bone to augment bone formation and bone mass. This new approach to increase the homing and retention of the MSCs to bone should now be examined in both preclinical and clinical studies for the treatment of osteoporosis and fracture repair.

METHODS

Methods and any associated references are available in the online version of the paper at http://www.nature.com/naturemedicine/.

Note: Supplementary information is available on the Nature Medicine website.

ACKNOWLEDGMENTS

The mouse MSCs used in this work were provided by the Texas A&M Health Science Center College of Medicine Institute for Regenerative Medicine at Scott & White through a grant from National Center for Research Resources of the US National Institutes of Health grant P40RR017447. This work was funded by the US National Institutes of Health grants NIAMS- 5R21AR057515 (to W.Y.), NIAM- R01AR043052 (to N.E.L.) and 1K12HD05195801 and was co-funded by the US National Institute of Child Health and Human Development (NICHD), the Office of Research on Women's Health (ORWH), the Office of Dietary Supplements (ODS) and the US National Institute of Aging (NIA).

AUTHOR CONTRIBUTIONS

W.Y., N.E.L. and K.S.L. designed the study. M.G. and W.Y. performed the animal study, collected data from the cell cultures, biochemistry, microCT and bone histomorphometry and analyzed all the data. R.L. and L.M. designed and synthesized the compound LLP2A-Ale. R.L. participated in the synthesis of LLP2A-Ale, and K.L. synthesized the LLP2A-Ale. J.N. and P.Z. performed human MSC cultures and designed the experiments using the NOD/SCID/MPSVII mice. J.J. and M.S. performed immunohistochemistry and helped with the animal studies. B. Panganiban and R.O.R. performed biomechanical testing and analyzed data. All authors edited the paper.

COMPETING FINANCIAL INTERESTS

The authors declare no competing financial interests.

Published online at http://www.nature.com/naturemedicine/.
Reprints and permissions information is available online at http://www.nature.com/reprints/index.html.

1. Stolzing, A., Jones, E., McGonagle, D. & Scutt, A. Age-related changes in human bone marrow-derived mesenchymal stem cells: consequences for cell therapies. *Mech. Ageing Dev.* **129**, 163–173 (2008).
2. Katsara, O. *et al.* Effects of donor age, gender, and *in vitro* cellular aging on the phenotypic, functional, and molecular characteristics of mouse bone marrow–derived mesenchymal stem cells. *Stem Cells Dev.* **20**, 1549–1561 (2011).
3. Bonyadi, M. *et al.* Mesenchymal progenitor self-renewal deficiency leads to age-dependent osteoporosis in Sca-1/Ly-6A null mice. *Proc. Natl. Acad. Sci. USA* **100**, 5840–5845 (2003).
4. Zhang, Y. *et al.* A nerve graft constructed with xenogeneic acellular nerve matrix and autologous adipose-derived mesenchymal stem cells. *Biomaterials* **31**, 5312–5324 (2010).
5. Pedram, M.S. *et al.* Transplantation of a combination of autologous neural differentiated and undifferentiated mesenchymal stem cells into injured spinal cord of rats. *Spinal Cord* **48**, 457–463 (2010).
6. Li, H., Yan, F., Lei, L., Li, Y. & Xiao, Y. Application of autologous cryopreserved bone marrow mesenchymal stem cells for periodontal regeneration in dogs. *Cells Tissues Organs* **190**, 94–101 (2009).
7. Gutwald, R. *et al.* Mesenchymal stem cells and inorganic bovine bone mineral in sinus augmentation: comparison with augmentation by autologous bone in adult sheep. *Br. J. Oral Maxillofac. Surg.* **48**, 285–290 (2010).
8. Vertenten, G. *et al.* Evaluation of an injectable, photopolymerizable, and three-dimensional scaffold based on methacrylate-endcapped poly(D,L-lactide-co-epsilon-caprolactone) combined with autologous mesenchymal stem cells in a goat tibial unicortical defect model. *Tissue Eng. Part A* **15**, 1501–1511 (2009).
9. Halleux, C., Sottile, V., Gasser, J.A. & Seuwen, K. Multi-lineage potential of human mesenchymal stem cells following clonal expansion. *J. Musculoskelet. Neuronal Interact.* **2**, 71–76 (2001).
10. Longobardi, L. *et al.* Subcellular localization of IRS-1 in IGF-I–mediated chondrogenic proliferation, differentiation and hypertrophy of bone marrow mesenchymal stem cells. *Growth Factors* **27**, 309–320 (2009).
11. Chapel, A. *et al.* Mesenchymal stem cells home to injured tissues when co-infused with hematopoietic cells to treat a radiation-induced multi-organ failure syndrome. *J. Gene Med.* **5**, 1028–1038 (2003).
12. Granero-Moltó, F. *et al.* Regenerative effects of transplanted mesenchymal stem cells in fracture healing. *Stem Cells* **27**, 1887–1898 (2009).
13. Gao, J., Dennis, J.E., Muzic, R.F., Lundberg, M. & Caplan, A.I. The dynamic *in vivo* distribution of bone marrow-derived mesenchymal stem cells after infusion. *Cells Tissues Organs* **169**, 12–20 (2001).
14. Meyerrose, T.E. *et al. In vivo* distribution of human adipose-derived mesenchymal stem cells in novel xenotransplantation models. *Stem Cells* **25**, 220–227 (2007).
15. Cho, S.W. *et al.* Transplantation of mesenchymal stem cells overexpressing RANK-Fc or CXCR4 prevents bone loss in ovariectomized mice. *Mol. Ther.* **17**, 1979–1987 (2009).
16. Jürg, A. Gasser, L.C.C., Kamibayashi, L.K. Intravenously administered mesenchymal OVX-induced bone loss in distribution of labeled MSCs. *J. Bone Miner. Res.* **14**, 1 (1999).
17. Granero-Moltó, F. *et al.* Regenerative effects of transplanted mesenchymal stem cells in fracture healing. *Stem Cells* **27**, 1887–1898 (2009).
18. Owen, M. & Friedenstein, A.J. Stromal stem cells: marrow-derived osteogenic precursors. *Ciba Found. Symp.* **136**, 42–60 (1988).
19. Bruder, S.P., Fink, D.J. & Caplan, A.I. Mesenchymal stem cells in bone development, bone repair, and skeletal regeneration therapy. *J. Cell. Biochem.* **56**, 283–294 (1994).
20. Muraglia, A., Cancedda, R. & Quarto, R. Clonal mesenchymal progenitors from human bone marrow differentiate *in vitro* according to a hierarchical model. *J. Cell Sci.* **113**, 1161–1166 (2000).
21. Adams, G.B. *et al.* Stem cell engraftment at the endosteal niche is specified by the calcium-sensing receptor. *Nature* **439**, 599–603 (2006).
22. Chen, X.D., Dusevich, V., Feng, J.Q., Manolagas, S.C. & Jilka, R.L. Extracellular matrix made by bone marrow cells facilitates expansion of marrow-derived mesenchymal progenitor cells and prevents their differentiation into osteoblasts. *J. Bone Miner. Res.* **22**, 1943–1956 (2007).

23. Grzesik, W.J. & Robey, P.G. Bone matrix RGD glycoproteins: immunolocalization and interaction with human primary osteoblastic bone cells *in vitro*. *J. Bone Miner. Res.* **9**, 487–496 (1994).
24. Vukicevic, S., Luyten, F.P., Kleinman, H.K. & Reddi, A.H. Differentiation of canalicular cell processes in bone cells by basement membrane matrix components: regulation by discrete domains of laminin. *Cell* **63**, 437–445 (1990).
25. Gronthos, S., Simmons, P.J., Graves, S.E. & Robey, P.G. Integrin-mediated interactions between human bone marrow stromal precursor cells and the extracellular matrix. *Bone* **28**, 174–181 (2001).
26. Gronthos, S., Stewart, K., Graves, S.E., Hay, S. & Simmons, P.J. Integrin expression and function on human osteoblast-like cells. *J. Bone Miner. Res.* **12**, 1189–1197 (1997).
27. Brooke, G., Tong, H., Levesque, J.P. & Atkinson, K. Molecular trafficking mechanisms of multipotent mesenchymal stem cells derived from human bone marrow and placenta. *Stem Cells Dev.* **17**, 929–940 (2008).
28. Hamidouche, Z. *et al.* Priming integrin α5 promotes human mesenchymal stromal cell osteoblast differentiation and osteogenesis. *Proc. Natl. Acad. Sci. USA* **106**, 18587–18591 (2009).
29. Mukherjee, S. *et al.* Pharmacologic targeting of a stem/progenitor population *in vivo* is associated with enhanced bone regeneration in mice. *J. Clin. Invest.* **118**, 491–504 (2008).
30. Peng, L. *et al.* Combinatorial chemistry identifies high-affinity peptidomimetics against α4β1 integrin for *in vivo* tumor imaging. *Nat. Chem. Biol.* **2**, 381–389 (2006).
31. Luo, J. *et al.* Rainbow beads: a color coding method to facilitate high-throughput screening and optimization of one-bead one-compound combinatorial libraries. *J. Comb. Chem.* **10**, 599–604 (2008).
32. Yao, W. *et al.* Inhibition of the progesterone nuclear receptor during the bone linear growth phase increases peak bone mass in female mice. *PLoS ONE* **5**, e11410 (2010).
33. Cao, J., Venton, L., Sakata, T. & Halloran, B.P. Expression of RANKL and OPG correlates with age-related bone loss in male C57BL/6 mice. *J. Bone Miner. Res.* **18**, 270–277 (2003).
34. Sato, M. *et al.* Abnormal bone architecture and biomechanical properties with near-lifetime treatment of rats with PTH. *Endocrinology* **143**, 3230–3242 (2002).
35. Dao, M.A., Taylor, N. & Nolta, J.A. Reduction in levels of the cyclin-dependent kinase inhibitor p27(kip-1) coupled with transforming growth factor beta neutralization induces cell-cycle entry and increases retroviral transduction of primitive human hematopoietic cells. *Proc. Natl. Acad. Sci. USA* **95**, 13006–13011 (1998).
36. Seeman, E. Periosteal bone formation—a neglected determinant of bone strength. *N. Engl. J. Med.* **349**, 320–323 (2003).
37. Kumar, S. & Ponnazhagan, S. Bone homing of mesenchymal stem cells by ectopic α4 integrin expression. *FASEB J.* **21**, 3917–3927 (2007).

ONLINE METHODS

Synthesis of LLP2A-Ale. The LLP2A-Ale was synthesized by Michael addition of the sulfhydryl group of LLP2A-Lys(D-Cys) to alendronate-maleimide (Ale-Mal). The synthetic scheme is shown in **Supplementary Figure 1**. Specifically, the peptidomimetic section, LLP2A-Lys(D-Cys), was synthesized to have a D-cysteine (D-Cys) attached to the side chain amino group of lysine (Lys) and to have a pair of identical hydrophilic linkers in series between the peptidomimetic ligand, LLP2A and the dipeptide Lys(D-Cys). This synthesis was performed on rink amide 4-methyl-benzhydrylamine (MBHA) resin using similar approaches as we previously reported[30]. Ale-Mal was prepared *in situ* from Ale and sulfosuccinimidyl-4-(*N*-maleimidomethyl)cyclohexane-1-carboxylate (sulfo-SMCC). In brief, Ale disodium salt (1.0 eq.) (powder from lyophilization of aqueous solution of alendronic acid and 2 eq. NaOH) was dissolved in 0.1 M PBS (with 10 mM EDTA), pH 7.5. The aqueous solution was then cooled in an ice water bath, and a solution of Sulfo-SMCC (1.1 eq.) in water was added dropwise. After the completion of this addition, the resulting solution was allowed to warm to 20–25 °C while being stirred for 2 h. This solution was cooled before the dropwise addition of a solution of LLP2A-Lys(D-Cys) (1.0 eq.) in a small amount of 50% acetonitrile/water. The pH was adjusted to between 6 and 7 with aqueous $NaHCO_3$. The resulting mixture was stirred for 1 h and then allowed to warm to room temperature 20–22 °C. After a a negative Ellman test, the solution was lyophilized. The resulting powder was redissolved in a small amount of 50% acetonitrile/water and purified by Reverse Phase High Performance Liquid Chromatography (RP-HPLC) (C18 column). Buffer A was 0.5% acetic acid/H_2O. Buffer B was 0.5% acetic acid/acetonitrile. The collected eluent was lyophilized to give a white powder. The identity was confirmed with matrix-assisted laser desorption/ionization mass spectrometry. $[M+H]^+$ (molecular weight value): 1970.78 (calculated: 1970.88).

***In vitro* cell differentiation arrays of MSCs into osteogenic, chondrogenic or adipogenic lineages.** Mouse MSCs were obtained under a material transfer agreement between the University of California Davis and the Texas A&M Institute for Regenerative Medicine. These cells were a relatively pure population of stromal cells that were negative for CD11b, CD45 and CD34 and positive for CD29, CD31 and CD106. For osteogenic differentiation, the passage-six mouse MSCs were used. On day 14 of the culture, a set of cells was used for RNA extraction and RT-PCR for the osteoblast gene markers *Runx2* and *Bglap*. At day 21 of the culture, another set of cells was stained with 0.2% crystal violet in 2% ethanol and photographed. The number of purple-stained colonies bigger than 1 mm in diameter was recorded. The plates were then eluted with 0.2% Triton TX100. The total eluted solution was run in a spectrophotometer at 590-nm absorbance. The same set of plates was then stained with Alizarin Red to monitor the formation of mineralization nodules. For the chondrogenesis micromass culture, the MSCs were cultured using a STEMPRO Chondrogenesis Differentiation Kit (GIBCO Invitrogen Cell Culture) and stained with Alcian Blue. For adipogenesis differentiation, the MSCs were cultured using a STEMPRO Adipogenesis Differentiation Kit (GIBCO Invitrogen Cell Culture) and stained with Oil Red O for the visualization of lipoid deposits.

***In vitro* migration assays for migration of mouse BMSCs.** Cell migration assays were performed using Transwell migration chambers (with a diameter of 6.5 mm and a pore size of 8 μm; Corning) coated with 0.5 μg ml^{-1} type-I collagen. The coated filters were placed into the lower chamber, which contained serum-free medium supplemented with 45 nM LLP2A-Ale. BMSCs were added to the upper compartment of the Transwell chamber and allowed to migrate to the underside of the top chamber for 10 h. None of the migrated cells on the upper membrane were removed, and the migrated cells were fixed, stained with crystal violet and counted. Subsequently, stained cells were eluted from membranes, and absorbance measurements were performed using an optical density of 590 nm. Experiments were performed in triplicate.

huMSC cultures. Bone marrow aspirates from human healthy donors were purchased from Lonza. Bone marrow aspirates were passed through 70 μm cell strainers, and the bone spicules that were retained on the cell strainers were collected. The pass-through was diluted with an equal volume of PBS and centrifuged over Ficoll for 30 min at 700*g*. Next, mononuclear cells and bone spicules were plated in plastic culture flasks using Minimal Essential Medium Alpha (HyClone Thermo Scientific) supplemented with 10% FBS (Atlanta Biologicals). After 2 d of culture, nonadherent cells were removed by 2 or 3 washing steps with PBS. MSCs from passage six were used for this experiment[14].

Histochemical analyses of enzyme activity. After the mice were euthanized, small portions of their organs were harvested and frozen in Optimal Cutting Temperature embedding media (Sakura) and cut into 12-μm sections. A glucuronidase, β (GUSB)-specific histochemical analysis was performed using naphthol-AS-BI-β-D-glucuronide (Sigma-Aldrich) as a substrate, which was followed by counterstaining with methyl green[14].

Animal treatments and other technical methods. All mice were treated according to the US Department of Agriculture animal care guidelines with the approval of the University of California Davis Committee on Animal Research. We previously published the methods for microCT, biochemical markers of bone turnover, bone histomorphometry, immunohistochemistry and biomechanical testing[38–40].

Statistics. The group means and s.d. were calculated for all outcome variables. Repeated measures analysis of variance was used to evaluate parameters derived from repeated *in vivo* microCT scans, such as the trabecular bone volume (BV/TV), and Bonferroni *post hoc* tests were used to compare time (age)-dependent changes within the same treatment group or between treatment groups at the same time point. The nonparametric Kruskal-Wallis test was used to determine differences between the groups for the other outcome measures obtained at the end of the studies (SPSS Version 12, SPSS). Differences were considered significant at $P < 0.05$.

38. Parfitt, A.M. *et al.* Bone histomorphometry: standardization of nomenclature, symbols, and units. Report of the ASBMR Histomorphometry Nomenclature Committee. *J. Bone Miner. Res.* **2**, 595–610 (1987).
39. Yao, W. *et al.* Glucocorticoid-induced bone loss in mice can be reversed by the actions of parathyroid hormone and risedronate on different pathways for bone formation and mineralization. *Arthritis Rheum.* **58**, 3485–3497 (2008).
40. Yao, W. *et al.* Overexpression of secreted frizzled-related protein 1 inhibits bone formation and attenuates parathyroid hormone bone anabolic effects. *J. Bone Miner. Res.* **25**, 190–199 (2010).